RAA 2021 Vol. **21** No. **4**, 103(8pp) doi: 10.1088/1674-4527/21/4/103

http://www.raa-journal.org *http://iopscience.iop.org/raa*

Research in Astronomy and Astrophysics

An explanation about the flat radio spectrum for Mrk 421

Rui Xue[1] and Ze-Rui Wang[2★]

[1] Department of Physics, Zhejiang Normal University, Jinhua 321004, China
[2] School of Astronomy and Space Science, Nanjing University, Nanjing 210093, China; *zerui_wang62@163.com*

Received 2020 September 22; accepted 2020 November 12

Abstract It is well known that a flat radio spectrum is a common property in the spectral energy distribution of blazars. Although one-zone leptonic models are generally successful in explaining the multi-wave band emission, they are problematic in reproducing the radio spectrum. In the study of Mrk 421, one-zone models suggest that in order to avoid overproducing the radio flux, the minimum electron Lorentz factor should be larger than a few hundred at least, even considering the synchrotron self-absorption effect. This result suggests that the model predicted spectral index in the radio band of Mrk 421 should be -1/3. On the basis of this result, by assuming there is a neglected region that will also contribute the radio emission and its electron energy index naturally originates from the simplest first-order Fermi acceleration mechanism, we can get a superimposed flat radio spectrum. In this paper, a two-zone model is proposed to reproduce the quiescent state spectral energy distribution of Mrk 421. In addition to taking into account the emission from a conventional radiation zone, we further consider emission from the acceleration zone in which particles are accelerated at a shock front. With the present model, our fitting result suggests that the low frequency flat radio spectrum of Mrk 421 might be explained as a superposition of the synchrotron emission from acceleration zone and radiation zone.

Key words: galaxies: active — galaxies: jets — radiation mechanisms: non-thermal

1 INTRODUCTION

Blazars, including flat-spectrum radio quasars (FSRQs) and BL Lacertae objects (BL Lacs), are radio-loud active galactic nuclei (AGNs) observed with their relativistic jet axis along the line of sight (Urry & Padovani 1995; Ulrich et al. 1997). FSRQs and BL Lacs are defined according to the presence or absence of strong broad-emission lines (Urry & Padovani 1995; Scarpa & Falomo 1997). The broadband spectral energy distribution (SED) of blazars has been quite well studied over all accessible energy bands (Madejski & Sikora 2016; Tan et al. 2020). In the logν-logνF_ν diagram, the typical SED of a blazar displays a double hump structure. In the leptonic model, it is generally accepted that the low energy hump originates from the synchrotron emission of relativistic electrons in the jet, and high energy hump is derived from inverse Compton (IC) scattering. However, the origin of the scattered photons has not yet been clearly identified. If soft photons are derived from synchrotron emission, the IC scattering is called the synchrotron self-Compton (SSC) process (Rees 1967; Jones et al. 1974; Marscher & Gear 1985; Maraschi et al. 1992; Sikora et al. 1994; Bloom & Marscher 1996); If soft photons are derived from the exterior of jets, the IC scattering is called the external Compton process (EC). In the latter case, soft photons can be produced directly by the accretion disk (Dermer et al. 1992; Dermer & Schlickeiser 1993) or indirectly, for instance, those reprocessed by the broad line region (Sikora et al. 1994; Dermer et al. 1997), or by the dust torus (Błażejowski et al. 2000; Arbeiter et al. 2002). In hadronic models, the high-energy bump originates from proton-synchrotron emission or emission from secondary particles (Aharonian 2000; Xue et al. 2019b), and the generated high-energy neutrino emission might be observed (e.g., Xue et al. 2019a, 2021).

Observationally, there is a break ($\nu_{\rm break}\sim10^{11}$ Hz) in the standard radio spectrum of blazars. In the high frequency region ($\nu > \nu_{\rm break}$), the radio spectrum steepens, signaling that the jet emission is optically thin. In the low frequency region ($\nu < \nu_{\rm break}$), most blazars display a flat spectrum, which is likely to be self-absorbed (and thus optically thick) (Blandford & Königl 1979;

★ Corresponding author

Ghisellini et al. 1985; Marscher 2009). On the other hand, there are some blazars that do not have a significant break in the radio spectrum (e.g., see the SEDs of J0006-0623, J0102+5824, J0433+0521 in Planck Collaboration et al. 2011). Statistically, the distributions of low frequency spectral indices are similar for FSRQs and BL Lacs with $\alpha\sim$-0.1, which mean that the flat radio spectrum is a common property for both types of blazars (Planck Collaboration et al. 2011; Giommi et al. 2012).

In order to explain this flat radio spectrum, many studies endeavor to reproduce it with an inhomogeneous model (Blandford & Königl 1979; Marscher 1980; Konigl 1981; Kaiser 2006; Pe'er & Casella 2009; Potter & Cotter 2012, 2013a,b,c, 2015). A jet model with a uniform conical structure was firstly proposed by Blandford & Königl (1979). Assuming that the magnetic luminosity is conserved in each segment, the flat radio spectrum is reproduced by a superposition of synchrotron self-absorbed radiation from each segment along the jet. However, the adiabatic losses are treated as optional in the standard Blandford-Königl jet model. When considering adiabatic loss, the re-acceleration of electrons must exist so that the adiabatic energy loss rate is balanced by the electron re-acceleration rate (Kaiser 2006; Potter & Cotter 2013a, 2015; Zdziarski et al. 2019), otherwise the flat radio spectrum remains unexplained.

From the perspective of the one-zone homogeneous model which is widely applied in blazar research, although the SEDs of blazars can be reproduced successfully (Ghisellini et al. 2011; Lister et al. 2011; Zhang et al. 2012; Yan et al. 2014; Zhang et al. 2014; Chen 2018; Tan et al. 2020), the flat radio spectrum cannot be fitted in most cases. From the SEDs that are fitted by the one-zone models, one can find that the observed radio flux is higher than the model predicted flux which considers self-absorption. Many studies suggest that the low frequency flat radio emission must come from a large-scale jet which is a larger and less compact region, therefore the one-zone homogeneous leptonic model that aims to explain the compact jet radiation cannot explain the low frequency radio emission (Ghisellini et al. 2009, 2010). However such explanations may be arbitrary, and the extended radiation from large-scale jets is different from the beamed core emission, and usually exhibits a steep spectrum at low frequencies (e.g., see fig. 1 in Meyer et al. 2011). In radio observation, the observed steep spectrum, rather than the flat spectrum, is also regarded as the basis for judging whether the emission comes from a large-scale area (e.g., Zhao et al. 2015). Therefore it cannot be simply considered that the unexplained flat radio spectrum of a one-zone model originates from the extended large-scale jet.

In this paper, without considering the emission from an extended region, we investigate the possibility that the emission associated with a flat spectrum could also come from the acceleration region, which has not been discussed in previous studies. In this case, even if the synchrotron emission of the radiation region is dominant in the low energy component, the acceleration region still has the potential to contribute emission at the radio band. Therefore, we propose a two-zone model in which particles are accelerated at a shock front and cooled via synchrotron and IC radiation in a homogeneous magnetic field behind it. In the following, we will discuss whether radiation from the acceleration zone could contribute the low frequency flat radio spectrum of a well-known blazar, Mrk 421. This paper is structured as follows. In Section 2 we present the model description; in Section 3 we model the SED of Mrk 421; in Section 4 we provide some discussions and conclusions.

2 MODEL DESCRIPTION

A two-zone scenario is proposed to explain the broadband emission in this paper. In the model, we basically follow Kirk et al. (1998) and reconsider the emission from the acceleration zone. We assume that the observed SED is a superposition of two zones that are radiating contemporaneously and boosted with the same Doppler factor (δ). We treat two zones: one around the shock front where the electrons are continuously accelerated from an initial value of the electron Lorentz factor γ_0 up to $\gamma_{\rm max}$ and then escape into a downstream region where electrons emit most of their radiation with an energy-independent rate $t_{\rm esc}^{-1}$. We assume a cylindrical geometry with the same constant cross-section for the two zones, and the length of the acceleration zone $L_{\rm acc}$ is relatively thinner than the length of the radiation zone $L_{\rm rad}$ (see Fig. 1). A brief description of the two-zone model is provided as follows (for more details, see Kirk et al. 1998).

Summing up all energy gain and loss terms, as well as electron injection and escape terms, we get the kinetic equation that governs the evolution of electrons in the acceleration zone

$$\frac{\partial N_{\rm acc}(\gamma,t)}{\partial t}+\frac{\partial}{\partial\gamma}[(\frac{\gamma}{t_{\rm acc}}-\beta_{\rm s}\gamma^2)N_{\rm acc}(\gamma,t)]+\frac{N_{\rm acc}(\gamma,t)}{t_{\rm esc}} = Q\delta(\gamma-\gamma_0), \tag{1}$$

where $N_{\rm acc}(\gamma,t)$ is the electron number density per γ in the acceleration zone, γ is the electron Lorentz factor, $t_{\rm acc}$ is the characteristic time for the shock acceleration gains, $\beta_{\rm s}\gamma^2=\frac{4\sigma_{\rm T}B^2\gamma^2}{3m_{\rm e}c8\pi}$ describes the synchrotron losses, $Q\delta(\gamma-\gamma_0)$ signifies the injection of monochromatic electrons with energy γ_0 into the acceleration process and $\delta(\gamma-\gamma_0)$ is the δ-function.

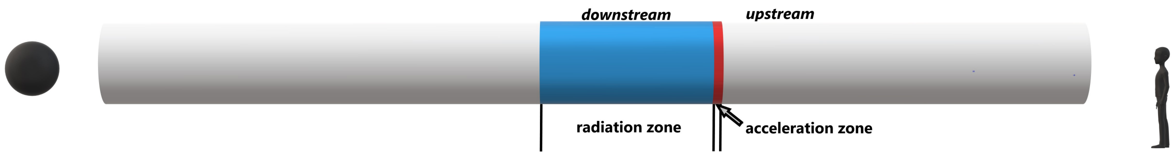

Fig. 1 A sketch, not to scale, of the two-zone model.

For $t > 0$ and $\gamma_0 < \gamma < \gamma_1(t)$, the solution of Equation (1) is given by

$$N_{\rm acc}(\gamma,t) = a\frac{1}{\gamma^2}(\frac{1}{\gamma} - \frac{1}{\gamma_{\rm max}})^{(t_{\rm acc}-t_{\rm esc})/t_{\rm esc}}, \quad (2)$$

where

$$\gamma_1(t) = (\frac{1}{\gamma_{\rm max}} + [\frac{1}{\gamma_0} - \frac{1}{\gamma_{\rm max}}e^{-t/t_{\rm acc}}])^{-1} \quad (3)$$

with $\gamma_{\rm max} = (\beta_{\rm s}t_{\rm acc})^{-1}$ and

$$a = Q_0 t_{\rm acc}\gamma_0^{t_{\rm acc}/t_{\rm esc}}(1 - \frac{\gamma_0}{\gamma_{\rm max}})^{-t_{\rm acc}/t_{\rm esc}}, \quad (4)$$

where Q_0 is a constant injection rate after switch-on at time t=0. $t_{\rm acc}$ and $t_{\rm esc}$ are assumed to be independent of energy here.

After being accelerated, electrons leave the acceleration zone at a rate $N_{\rm acc}(\gamma,t)/t_{\rm esc}$ and enter the radiation zone where they lose most of their energy via the synchrotron and IC processes. The evolution of electrons in the radiation zone is governed by the following kinetic equation

$$\frac{\partial N_{\rm rad}(\gamma,t)}{\partial t} - \frac{\partial}{\partial\gamma}((\beta_{\rm s}\gamma^2 + P_{\rm IC})N_{\rm rad}(\gamma,t)) = \frac{N_{\rm acc}(\gamma,t)}{t_{\rm esc}}\delta(x - x(t)), \quad (5)$$

where $N_{\rm rad}(\gamma,t)$ is the electron number density per γ in the radiation zone, $P_{\rm IC} = m_{\rm e}^3c^7h\int_0^{\xi_{\rm max}}d\xi\xi\int_0^{\infty}d\xi_1 N_{\rm ph}(\xi_1)\frac{N(\gamma,\xi_1)}{dtd\xi}$ describes the IC losses including the Klein-Nishina effect (Schlickeiser 2002), where $N_{\rm ph}$ is the differential photon number density, ξ and ξ_1 are the non-dimensional energies for the scattered photons and the target photons respectively, $x(t)$ is the position of the shock front at time t and $\delta(x - x(t))$ is the δ-function. Note that the acceleration term in Equation (1) is not considered here, since electrons only get accelerated in the acceleration zone in this model.

The kinetic equations for acceleration zone and radiation zone are solved for the time, space and energy dependences of the particle distribution function. Therefore, this two-zone model is homogeneous in the sense that the magnetic field does not vary, but contains an inhomogeneous electron energy distribution. On the other hand, by assuming the magnetic field intensity B for the two zones is the same, we can calculate their synchrotron emission coefficients through

$$j_{\rm syn}(\nu) = \frac{1}{4\pi}\int N_{\rm acc,rad}(\gamma)P(\nu,\gamma)d\gamma, \quad (6)$$

where $P(\nu,\gamma)$ is the mean emission coefficient for a single electron integrated over the isotropic distribution of pitch angles. Also, the synchrotron absorption coefficients for the acceleration zone and the radiation zone are calculated with

$$\alpha_{\rm syn}(\nu) = -\frac{1}{8\pi\nu^2 m}\int d\gamma P(\nu,\gamma)\gamma^2\frac{\partial}{\partial\gamma}[\frac{N_{\rm acc,rad}(\gamma)}{\gamma^2}]. \quad (7)$$

Then we can compute the synchrotron intensity utilizing the radiative transfer equation

$$I_{\rm syn}(\nu) = \frac{j_{\rm syn}(\nu)}{\alpha_{\rm syn}(\nu)}(1 - e^{-\alpha_{\rm syn}(\nu)L_{\rm acc,rad}}), \quad (8)$$

where $\alpha_{\rm syn}(\nu)L_{\rm acc,rad}$ is the optical depth.

The SSC emission coefficient is defined by

$$j_{\rm SSC} = \frac{h\epsilon}{4\pi}\int d\epsilon_0 n(\epsilon_0)\int\gamma N_{\rm acc,rad}(\gamma)C(\epsilon,\gamma,\epsilon_0), \quad (9)$$

where ϵ is the scattered photon energy and ϵ_0 is the soft photon energy. $C(\epsilon,\gamma,\epsilon_0)$ is the Compton kernel given by Jones (1968)

$$C(\epsilon,\gamma,\epsilon_0) = \frac{2\pi r_{\rm e}^2 c}{\gamma^2\epsilon_0}[2\kappa\ln(\kappa) + (1+2\kappa)(1-\kappa) + \frac{(4\epsilon_0\gamma\kappa)^2}{2(1+4\epsilon_0\gamma\kappa)}(1-\kappa)], \quad (10)$$

where

$$\kappa = \frac{\epsilon}{4\epsilon_0\gamma(\gamma-\epsilon)}, \quad (11)$$

and $n(\epsilon_0)$ is the number density of the synchrotron photons per energy interval.

Because the medium for the SSC radiation field is transparent, we can calculate the SSC intensity

$$I_{\rm SSC}(\nu) = j_{\rm SSC}(\nu)L_{\rm acc,rad}. \quad (12)$$

Then we can get the total observed flux density as

$$F_{\rm obs}(\nu_{\rm obs}) = \frac{\pi R^2\delta^3(1+z)}{D_{\rm L}^2}(I_{\rm syn}(\nu) + I_{\rm SSC}(\nu)), \quad (13)$$

where $D_{\rm L}$ is the luminosity distance, z is the redshift, $\nu_{\rm obs}$ = $\nu\delta/(1+z)$ and R is the radius of the cross-section. In addition, the very high energy (VHE) γ-ray photons will be absorbed by the extragalactic background light (EBL). It makes the observed spectrum in the VHE band steeper than the intrinsic one. According to the EBL model that was presented by Domínguez et al. (2011), we calculate the absorption in the GeV-TeV band.

3 APPLICATION

3.1 Modeling the SED of Mrk 421

The high synchrotron peak BL Lac Mrk 421, at a redshift of z = 0.03, is one of the brightest TeV blazars and has been investigated by many researchers (e.g. Abdo et al. 2011a). In the study of its SED, the conventional one-zone leptonic model suggests that in order to avoid predicting a larger radio flux than the observed data, the minimum Lorentz factor γ_0 should be much larger than the typical value which is in the range between 1 and 100 (Celotti & Ghisellini 2008; Zhang et al. 2014). In the one-zone SSC model, Abdo et al. (2011a) set $\gamma_0 = 400, 800$, Aleksić et al. (2014) set $6000 < \gamma_0 < 17\,000$ and Yan et al. (2014) set $\gamma_0 = 500$. This implies that if γ_0 is large enough, the spectral index α_1 ($F_\nu \propto \nu^{-\alpha_1}$) in the radio band should be -1/3 which is contributed by the monochrome electron γ_0. Moreover, if the acceleration zone can also contribute to the radio emission and the electrons are accelerated through the simplest first-order Fermi acceleration mechanism, it will give a canonical value for α_2 of about 0.75 (Sironi et al. 2015). Then we can obtain a superimposed flat radio spectrum with $\alpha \approx 0.2$ ($\alpha \approx (\alpha_1+\alpha_2)/2$). Motivated by the above issues, in this paper, we employ a two-zone model that was presented in Section 2 to reproduce the broadband SED of Mrk 421 and investigate whether the acceleration zone could contribute flux in the radio band and stack the emission of the radiation zone to get the low frequency flat radio spectrum. The averaged SED of Mrk 421 resulting from quasi-simultaneous observations integrated over a period of 4.5 months is provided by Abdo et al. (2011a), which is the most complete SED ever collected for Mrk 421. This averaged SED is a good proxy for the quiescent state because of its low activity and relatively low variability (Paneque & Fermi Large Area Telescope Collaboration 2010).

There are 11 parameters in the two-zone model, which are Q_0, R, $L_{\rm acc}$, $L_{\rm rad}$, B, δ, $t_{\rm acc}/t_{\rm esc}$, $t_{\rm obs}$, $\gamma_{0,\rm acc}$, $\gamma_{0,\rm rad}$ and $\gamma_{\rm max}$, respectively. As introduced in Section 2, $L_{\rm acc}$ and $L_{\rm rad}$ would affect the synchrotron and SSC intensities, and $L_{\rm acc}$ should be relatively thinner than $L_{\rm rad}$. In this work, the acceleration mechanism is not specified, but we assume the Fermi-type acceleration mechanism operates. In order to accelerate the particles effectively, the mean free path between clouds of plasma should be smaller than $L_{\rm acc}$. Here, we further assume that $L_{\rm acc}$ is ten times the mean free path between clouds of plasma. The mean free path between clouds of plasma can be estimated as $L = \frac{4v^2 t_{\rm acc}}{3c}$ (Park & Petrosian 1995), where $t_{\rm acc} = 1/(\gamma_{\rm max}\beta_{\rm s})$ and $v = 0.1\,c$ is the velocity of clouds of plasma relative to the particles. The model is not sensitive to the parameter $\gamma_{\rm max}$, so we set $\gamma_{\rm max} = 2\times10^6$ in this work. Then we can get $L = 2.16\times10^{15}\,{\rm cm}$ and $L_{\rm acc} = 2.16\times10^{16}\,{\rm cm}$. Following previous studies, we set $\gamma_{0,\rm acc} \approx 48$ in the modeling (Zhang et al. 2014). If assuming that the upstream electrons move in the opposite direction with an upstream Lorentz factor $\gamma_{0,\rm acc}$, $\gamma_{0,\rm rad}$ can be calculated according to the relativistic superposition (Weidinger et al. 2010),

$$\begin{aligned}\gamma_{0,\rm rad} &= [1-(\frac{\sqrt{\Gamma^2-1}\Gamma+\sqrt{\gamma_{0,\rm acc}^2-1}\gamma_{0,\rm acc}}{\Gamma^2+\gamma_{0,\rm acc}^2-1})^2]^{-1/2}\\ &= 2.3\times10^3.\end{aligned} \tag{14}$$

Finally, there are seven free parameters in our SED fitting. The minimum χ^2 technique is applied to perform the SED fits. For the radio and optical data with no reported uncertainties, we take 1% of the observed flux as the error. For the ultraviolet (UV) and X-ray data with no reported uncertainties, we take 2% of the observed flux as the error (Zhang et al. 2012; Aleksić et al. 2014). The fitting result of Mrk 421 is plotted in Figure 2. The red dotted line represents synchrotron emission in the acceleration zone. The green dashed line signifies synchrotron and SSC emission in the radiation zone. The yellow solid line corresponds to the total spectrum by summing both the acceleration zone and radiation zone emission. The model parameters used for the fitting and the values of χ^2 are expressed in Table 1. The columns in Table 1 are as follows: (1) source name; (2) redshift; (3) the constant injection rate in the unit of ${\rm cm^{-2}\,s^{-1}}$; (4) the magnetic field in the unit of G; (5) the radius of the cross-section in the unit of cm; (6) the length of the radiation zone in the unit of cm; (7) time of observation in the unit of s; (8) the Doppler factor; (9) $t_{\rm acc}/t_{\rm esc}$; (10) the value of χ^2.

From Figure 2, we can see that the full-waveband observation data of Mrk 421 is reproduced well, including the flat radio spectrum. Figure 2 affirms that the emission beyond 10^{11} Hz is dominated by the radiation zone, but the only contribution from the acceleration zone is between 10^9 Hz and 10^{11} Hz. This result suggests that the synchrotron radio emission ($\nu > 10^9$ Hz) in the acceleration zone is optically thin and the low frequency

Table 1 Model parameters.

Source name	z	Q_0 ($\mathrm{cm^{-2}s^{-1}}$)	B (G)	R (cm)	$L_{\rm rad}$ (cm)	$t_{\rm obs}$ (s)	δ	$t_{\rm acc}/t_{\rm esc}$	χ^2
Mrk 421	0.03	8.90×10^8	0.012	1.41×10^{17}	1.06×10^{18}	2.4×10^7	24	1.4	1.28

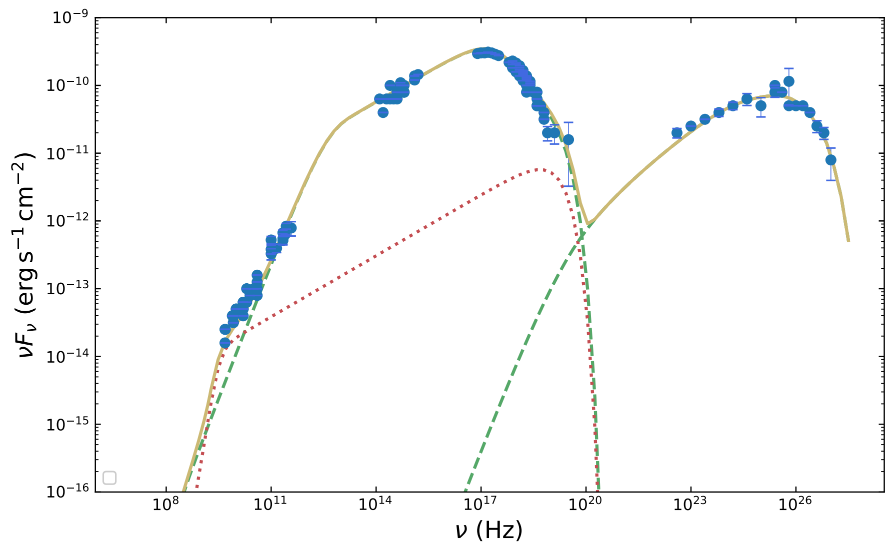

Fig. 2 The two-zone SSC model for SED modeling of Mrk 421. The red dotted line represents synchrotron emission in the acceleration zone. The green dashed line signifies synchrotron and SSC emission in the radiation zone. The yellow solid line corresponds to the total spectrum by summing both the acceleration zone and radiation zone emission.

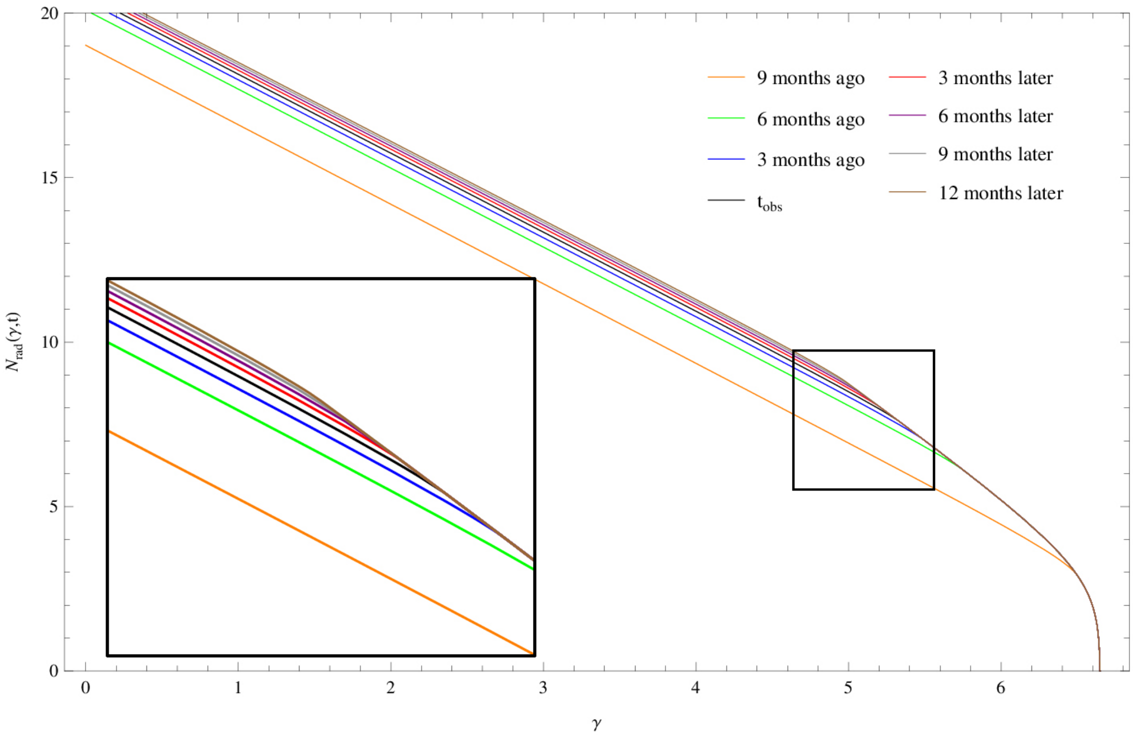

Fig. 3 The electron energy distribution in the radiation zone at different times. It can be seen that the electron energy distribution does not evolve significantly at large times and it is reasonable to treat our electron energy distribution that is observed at $t_{\rm obs}$ as steady state.

flat radio spectrum can be explained by the superposition of the two-zone synchrotron emission self-consistently.

3.2 Evolution of the electron energy distribution in the radiation zone

The multi-frequency data were collected during a 4.5 month campaign, and display low activity at all frequencies during this period (Abdo et al. 2011a). It means that the electron energy distribution is closer to steady state in this period. Moreover, in Figure 2 we can find that almost all the emission is dominated by the radiation zone. The electron energy distribution in the radiation zone can be solved by Equation (5) and the solution is a time-dependent function. This time-dependent two-zone model applied in this work is also used to study the multi-wavelength variabilities of some blazars (Weidinger & Spanier 2010). As is well known, Mrk 421 is a highly variable blazar, and this work focuses on studying the origin of the radio spectrum in a quiescent state. Therefore it is valuable to examine the evolution of the electron energy distribution over time and figure out whether the electron energy distribution at $t_{\rm obs}$ is in steady state or in variable state. According to the parameters that are constrained by the χ^2 fitting, the model predicted SED of Mrk 421 is observed at $t_{\rm obs} = 2.4 \times 10^7$ s. The electron energy distributions at $t_{\rm obs}$, $t_{\rm obs} \pm 3$ months, $t_{\rm obs}\pm6$ months, $t_{\rm obs}\pm9$ months and $t_{\rm obs}+12$ months are presented in Figure 3. As can be seen, as time increases, the electron energy distribution is getting closer to steady state. We find that the electron energy distribution has already begun to be close to steady state at $t_{\rm obs}$-6 months in our model. This result suggests that the electron energy distribution does not evolve significantly at large times and it is reasonable to treat our electron energy distribution that is observed from $t_{\rm obs}$-6 months to $t_{\rm obs}$+12 months as steady state. This period is much longer than 4.5 months. It means that our model is consistent with the observational result during the multi-frequency campaign.

4 DISCUSSION AND CONCLUSION

As a common property, most blazars show a flat spectrum in the low frequency radio band. For spectral index, many studies adopt $\alpha = 0$ for the low frequency radio band (Cheng et al. 2000; Donato et al. 2001; Abdo et al. 2010; Xiong et al. 2013). A statistical study of the radio spectrum of extragalactic radio sources is presented in Planck Collaboration et al. (2011). Their results suggest that the distribution of low frequency spectral indices is narrow and nearly 91% of indices are in the range α = –0.5 $\sim$ 0.5. As expected, their results suggest that the low frequency radio spectrum is flat with an average value of 0.06.

As one of the challenges, it is difficult for the one-zone leptonic model to explain the flat radio spectrum. There is, however, disagreement concerning the explanation of the flat radio spectrum. (1) It comes from a large-scale jet. However, the extended radio emission from the large-scale jet should display a steep spectrum, but not a flat spectrum (Punsly 1995; Meyer et al. 2011; Zhao et al. 2015). (2) Some researchers believe that the flat radio spectrum results from the superposition of many self-absorbed synchrotron components with different turnover frequencies in the inner parts of jets (Kellermann & Pauliny-Toth 1969; Usher et al. 1983; Planck Collaboration et al. 2011). (3) Some studies suggest that inhomogeneous models can explain the flat radio spectrum (Marscher 1980; Konigl 1981; Ghisellini et al. 1985; Potter & Cotter 2012).

From a phenomenal perspective, it is much simpler for the direct contribution from one additional region or the superposition of this additional region and a compact blob to form the flat radio spectrum. In the radio observation of an AGN, the extended radio emission could have a significant contribution that may dominate over the radio emission from the inner jet. However, Pei et al. (2016) ascertained that the radio core dominance of Mrk 421 is 0.84, which suggests that the flux of radio core emission is about one order of magnitude higher than that of the extended radio emission. Therefore, the contribution of the extended region to the observed radio spectrum is minor, and we have not considered it in this work. On the basis of the one-zone model, we further consider the contribution of the acceleration zone around the shock front to the observed SED. In this work, we present a two-zone model to fit the broadband SED of Mrk 421 in the steady state. From our fitting result, we suggest that the low frequency flat radio spectrum of Mrk 421 can be explained as a superposition of synchrotron emission from the acceleration zone and radiation zone. Among them, the contribution from the acceleration zone comes from its steep radio spectrum, and the contribution from the radiation zone arises from its radio spectrum with $\alpha_{\rm rad} = -1/3$. As the spectral index of the steep radio spectrum in the acceleration zone is the same as the steep radio spectrum in the radiation zone, we can study it through the observed radio spectrum. Giommi et al. (2012) examine the low and high frequency radio spectrum with a power law to estimate their spectral indices of 105 blazars. The average values of the high frequency spectral indices ($\alpha_{\rm HF}$, for $\nu > \nu_{\rm break}$) of FSRQs and BL Lacs are $\alpha_{\rm HF} = 0.73 \pm 0.04$ and $\alpha_{\rm HF} = 0.51 \pm 0.07$, respectively. The $\alpha_{\rm HF} = 0.73 \pm 0.04$ for FSRQs emerges naturally from the simplest first-order Fermi acceleration mechanism and the $\alpha_{\rm HF} = 0.51 \pm 0.07$ for BL Lacs is in agreement with the simplest diffusive shock acceleration models (Bednarz & Ostrowski 1998; Rieger et al. 2007). By superimposing the spectrum from the radiation zone with $\alpha_{\rm rad}$ = -1/3 and the steep spectrum from the acceleration zone that can be explained by the acceleration mechanisms, we can obtain the low frequency flat radio spectrum with spectral indices ($\alpha_{\rm LF}$, for $\nu < \nu_{\rm break}$) of $\alpha_{\rm LF} \approx 0.2$ for FSRQs and $\alpha_{\rm LF} \approx 0.08$ for BL Lacs. This result is consistent with the statistical average value of 0.1 that is presented by Giommi et al. (2012) which suggests that our model can explain the low frequency flat radio spectrum self-consistently.

As introduced in Section 3.1, when considering the upstream electrons moving in the opposite direction, $\gamma_{0,\rm rad}$ is much higher than $\gamma_{0,\rm acc}$. Moreover, we suggest that the difference between $\gamma_{0,\rm rad}$ and $\gamma_{0,\rm acc}$ may imply some physical mechanisms worked in the shock. The energy dissipation mechanisms operating at the shock fronts do introduce a particular characteristic (injection) energy scale, below which the particles are not freely able to cross the shock front and enter the radiation zone (Abdo et al. 2011b). Such a scale depends critically on the ratio of number of leptons to protons in the shocked plasma (q) and the fraction of the shock energy that is transferred to the acceleration of leptons ($\epsilon_{\rm e}$) (Inoue & Tanaka 2016)

$$E_{\rm c} = \Gamma m_{\rm p} c^2 \frac{\epsilon_{\rm e}}{q} \frac{p-2}{p-1}, \tag{15}$$

where $E_{\rm c} = \gamma_{0,\rm rad} m_{\rm e} c^2$, $p \approx 2.58$ is the spectral index derived in the modeling and $\Gamma = \delta = 24$[1]. We consider the jet to be electrically neutral, and the number of electrons and protons is approximately equal ($q \approx 1$), so we can get the value $\epsilon_{\rm e} \approx 0.14$. It means that 14% of the shock energy goes into electron acceleration which is consistent with the value (10%) that was obtained in Abdo et al. (2011b) and Inoue & Tanaka (2016).

As a conclusion, we propose an alternative interpretation of the low frequency flat radio spectrum of Mrk 421. The fitting result shows that almost all the emission is still dominated by the radiation zone. However, in the radio band, both the acceleration zone and the radiation zone can contribute to the radio flux. Our model also suggests that the flat radio emission of the jet in Mrk 421 originated from a compact cylindrical region rather than a large scale region. On the other hand, the two-zone model that is presented in this paper still requires improvements. For example, the length of the radiation zone is sufficiently long that we can consider energy conservation, bulk acceleration and electron continuity along the jet. Among them, only electron continuity from the acceleration zone to the tail of the radiation zone is taken into account in the two-zone model. In addition, the two-zone model can only reproduce a relatively narrow region of a flat radio spectrum. In order to explain the general properties of a low frequency flat radio spectrum over a larger and varying range, a more complex radiation model should be expected.

[1] For a relativistic jet close to the line of sight in blazars with a viewing angle of $\theta \lesssim 1/\Gamma$, we have $\delta = [\Gamma(1-\beta\cos\theta)]^{-1} \approx \Gamma$.

Acknowledgements We thank the anonymous referee for insightful comments and constructive suggestions. This work is supported by the Ph.D. Research start-up fund of Zhejiang Normal University (Grant No. YS304320082).

References

Abdo, A. A., Ackermann, M., Agudo, I., et al. 2010, ApJ, 716, 30
Abdo, A. A., Ackermann, M., Ajello, M., et al. 2011a, ApJ, 736, 131
Abdo, A. A., Ackermann, M., Ajello, M., et al. 2011b, ApJ, 727, 129
Aharonian, F. A. 2000, New Astron., 5, 377
Aleksić, J., Ansoldi, S., Antonelli, L. A., et al. 2014, A&A, 567, A135
Arbeiter, C., Pohl, M., & Schlickeiser, R. 2002, A&A, 386, 415
Bednarz, J., & Ostrowski, M. 1998, Phys. Rev. Lett., 80, 3911
Blandford, R. D., & Königl, A. 1979, ApJ, 232, 34
Błażejowski, M., Sikora, M., Moderski, R., & Madejski, G. M. 2000, ApJ, 545, 107
Bloom, S. D., & Marscher, A. P. 1996, ApJ, 461, 657
Celotti, A., & Ghisellini, G. 2008, MNRAS, 385, 283
Chen, L. 2018, ApJS, 235, 39
Cheng, K. S., Zhang, X., & Zhang, L. 2000, ApJ, 537, 80
Dermer, C. D., & Schlickeiser, R. 1993, ApJ, 416, 458
Dermer, C. D., Schlickeiser, R., & Mastichiadis, A. 1992, A&A, 256, L27
Dermer, C. D., Sturner, S. J., & Schlickeiser, R. 1997, ApJS, 109, 103
Domínguez, A., Primack, J. R., Rosario, D. J., et al. 2011, MNRAS, 410, 2556
Donato, D., Ghisellini, G., Tagliaferri, G., & Fossati, G. 2001, A&A, 375, 739
Ghisellini, G., Maraschi, L., & Treves, A. 1985, A&A, 146, 204
Ghisellini, G., Tavecchio, F., & Ghirlanda, G. 2009, MNRAS, 399, 2041
Ghisellini, G., Tavecchio, F., Foschini, L., et al. 2010, MNRAS, 402, 497
Ghisellini, G., Tavecchio, F., Foschini, L., & Ghirland a, G. 2011, MNRAS, 414, 2674
Giommi, P., Polenta, G., Lähteenmäki, A., et al. 2012, A&A, 541, A160
Inoue, Y., & Tanaka, Y. T. 2016, ApJ, 828, 13
Jones, F. C. 1968, Physical Review, 167, 1159
Jones, T. W., O'dell, S. L., & Stein, W. A. 1974, ApJ, 188, 353
Kaiser, C. R. 2006, MNRAS, 367, 1083

Kellermann, K. I., & Pauliny-Toth, I. I. K. 1969, ApJL, 155, L71
Kirk, J. G., Rieger, F. M., & Mastichiadis, A. 1998, A&A, 333, 452
Konigl, A. 1981, ApJ, 243, 700
Lister, M. L., Aller, M., Aller, H., et al. 2011, ApJ, 742, 27
Madejski, G. G., & Sikora, M. 2016, ARA&A, 54, 725
Maraschi, L., Ghisellini, G., & Celotti, A. 1992, ApJL, 397, L5
Marscher, A. P. 1980, ApJ, 235, 386
Marscher, A. P. 2009, arXiv e-prints, arXiv:0909.2576
Marscher, A. P., & Gear, W. K. 1985, ApJ, 298, 114
Meyer, E. T., Fossati, G., Georganopoulos, M., & Lister, M. L. 2011, ApJ, 740, 98
Paneque, D., & Fermi Large Area Telescope Collaboration. 2010, in Astronomical Society of the Pacific Conference Series, 427, Accretion and Ejection in AGN: a Global View, eds. L. Maraschi, G. Ghisellini, R. Della Ceca, & F. Tavecchio, 277
Park, B. T., & Petrosian, V. 1995, ApJ, 446, 699
Pe'er, A., & Casella, P. 2009, ApJ, 699, 1919
Pei, Z.-Y., Fan, J.-H., Liu, Y., et al. 2016, Ap&SS, 361, 237
Planck Collaboration, Aatrokoski, J., Ade, P. A. R., et al. 2011, A&A, 536, A15
Potter, W. J., & Cotter, G. 2012, MNRAS, 423, 756
Potter, W. J., & Cotter, G. 2013a, MNRAS, 429, 1189
Potter, W. J., & Cotter, G. 2013b, MNRAS, 431, 1840
Potter, W. J., & Cotter, G. 2013c, MNRAS, 436, 304
Potter, W. J., & Cotter, G. 2015, MNRAS, 453, 4070
Punsly, B. 1995, AJ, 109, 1555
Rees, M. J. 1967, MNRAS, 137, 429
Rieger, F. M., Bosch-Ramon, V., & Duffy, P. 2007, Ap&SS, 309, 119
Scarpa, R., & Falomo, R. 1997, A&A, 325, 109
Schlickeiser, R. 2002, Cosmic Ray Astrophysics (Berlin: Springer. ISBN 3-540-66465-3)
Sikora, M., Begelman, M. C., & Rees, M. J. 1994, ApJ, 421, 153
Sironi, L., Keshet, U., & Lemoine, M. 2015, Space Sci. Rev., 191, 519
Tan, C., Xue, R., Du, L.-M., et al. 2020, ApJS, 248, 27
Ulrich, M.-H., Maraschi, L., & Urry, C. M. 1997, ARA&A, 35, 445
Urry, C. M., & Padovani, P. 1995, PASP, 107, 803
Usher, P. D., Huang, K. L., Mitchell, K. J., & Pollock, J. T. 1983, ApJ, 264, 451
Weidinger, M., Rüger, M., & Spanier, F. 2010, Astrophysics and Space Sciences Transactions, 6, 1
Weidinger, M., & Spanier, F. 2010, A&A, 515, A18
Xiong, D. R., Zhang, H. J., Zhang, X., et al. 2013, Ap&SS, 345, 345
Xue, R., Liu, R.-Y., Petropoulou, M., et al. 2019a, ApJ, 886, 23
Xue, R., Liu, R.-Y., Wang, X.-Y., Yan, H., & Böttcher, M. 2019b, ApJ, 871, 81
Xue, R., Liu, R.-Y., Wang, Z.-R., et al. 2021, ApJ, 886, 23
Yan, D., Zeng, H., & Zhang, L. 2014, MNRAS, 439, 2933
Zdziarski, A. A., Stawarz, Ł., & Sikora, M. 2019, MNRAS, 485, 1210
Zhang, J., Liang, E.-W., Zhang, S.-N., & Bai, J. M. 2012, ApJ, 752, 157
Zhang, J., Sun, X.-N., Liang, E.-W., et al. 2014, ApJ, 788, 104
Zhao, G.-Y., Chen, Y.-J., Shen, Z.-Q., Sudou, H., & Iguchi, S. 2015, AJ, 149, 46